Synthesis of Graphene by the Chemical Vapor Deposition method and the study of its electronic properties

Lokeshwar Bandhu

Thesis
Submitted Towards Partial Fulfillment
of
BS-MS Dual Degree Program

Under the guidance of

Dr. Mandar Deshmukh
Faculty Member
Deaprtment of Condensed Matter Physics and Material Science
Tata Institute of Fundamental Research
Mumbai, India

&

Prof. Sulabha Kulkarni
Professor, Physics
Deaprtment of Physics
Indian Institute of Science Education and Research
Pune, India

Department of Physics
Indian Institute of Science Education and Research Pune

April 2011

Certificate

This is to certify that this dissertation entitled "Synthesis of Graphene by the Chemical Vapor Deposition method and the study of its elctronic properties" submitted towards the partial fulfillment of the BS-MS Dual Degree Program at the Indian Institute of Science Education and Research, Pune, represents original research carried out by Lokeshwar Bandhu at the Department of Condensed Matter Physics and Material Science, Tata Institute of Fundamental Research, Mumbai under the supervision of Dr. Mandar Deshmukh during the academic year 2010-2011.

Name of the student: Lokeshwar Bandhu
Signature:

Supervisor
DR. MANDAR DESHMUKH

Date:
Place:

Head, Physical Sciences
PROF. K.N.GANESH

Date:
Place:

Acknowledgments

This project would not have been possible without the help of several people. Firstly, I would like to express my gratitude to Dr. Mandar Deshmukh who provided me this wonderful opportunity to explore this interesting and exciting project. It was a great learning experience. Secondly, I thank Prof. Sulabha Kulkarni for her guidance and constant support. She has been my mentor for the last 3 years. Her constant support and faith motivated me to believe in myself and work hard. My heartiest thanks to Vibhor, Shamashish, Sajal and Hari for patiently dealing with my numerous questions. It would have been very difficult without their valuable advice. No less thanks to my labmates who were of help. Lastly, I thank my family and my close friends who have endured me continually and whose unconditional belief in my potential as a scientific investigator was something that had always helped me to pick myself up even when the going got tough. I would especially like to thank my friends Sushant More, Anand Pathak, and Ajinkya for their moral support and technical help.

Abstract

This project was aimed at developing monolayer graphene by the Chemical Vapor Deposition (CVD) method and to study its electronic properties at room and low temperatures. In order to optimize the growth conditions for continuous monolayer graphene, growth has been done at different temperature and pressure. We have tried different cleaning protocols and etchants for getting clean graphene. In terms of the residues left after etching, sodium persulfate has proved to be a better etchant than ferric chloride. Over the CVD grown graphene the devices were fabricated using Electron Beam Lithography. By using the Hall-bar-type electrode configuration we measure magnetoresistances and Hall resistances in a transverse magnetic field. A gating effect is measured by applying gate voltage to the Si back gate. We characterized the electronic properties and the mobility of the devices have been found to be 7093 $cm^2V^{-1}s^{-1}$ for a device of area 88.26 μm^2 at 1.4 K.

Contents

Chapter 1

Introduction

1.1 What is graphene?

Graphene is a two dimensional flat monolayer of carbon atoms arranged in a honeycomb lattice. It is the basic building block for the graphitic materials of all dimensionalities (fullerenes, carbon nanotubes, graphite). Its discovery and the exceptional properties shown by the experiments using it has led to the Nobel Prize in Physics for the year 2010 to Andre Geim and K. Novoselov, University of Manchester, UK. It is an amazing material with incredible electronic and mechanical prop-

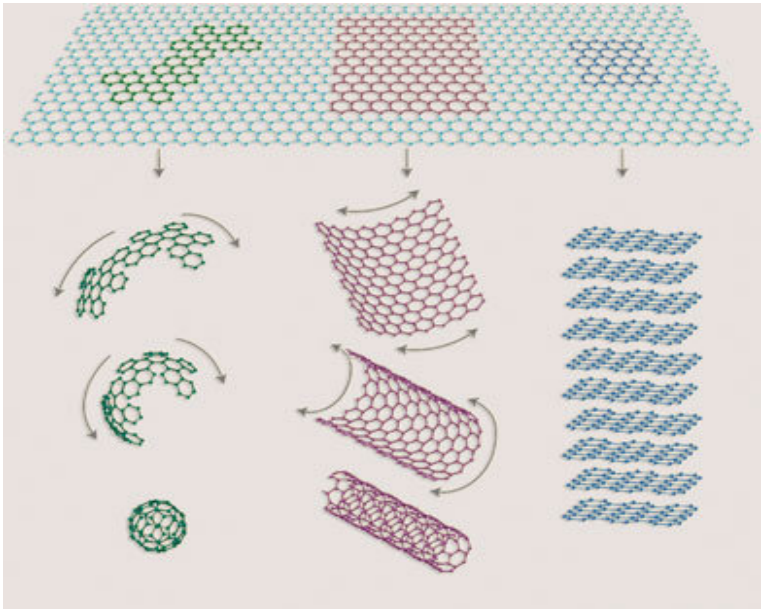

Figure 1.1: *Graphene is a 2D building material for carbon materials of all other dimensionalities(illustration taken from [1])*

erties. Before its discovery in 2004 by Andre Geim it was believed that strictly 2D crystals were thermodynamically unstable and could not exist and was considered of theoretical importance only [1]. The experiments on graphene confirmed that it is remarkable- stable, chemically inert, and crystalline under ambient conditions.

Its honeycomb lattice, with each carbon atom connected to its neighbours through strong covalent bonds, explains graphene's strength and rigidity.

1.1.1 Why study graphene?

Several reasons can be attributed to the current interest in graphene. Graphene films are found to be 2D and semi-metallic, with minimum overlap between conduction and valence bands. They exhibit a strong ambi-polar electric field effect with electrons and holes in concentrations up to 10^{13} cm^{-2}. It is believed that their mobilities (μ) can be improved upto 100,000 cm^{2}V^{-1}s^{-1} [1]. Interestingly, the charge carriers in graphene mimic relativistic particles. Thus, they are more easily described by the Dirac equation rather than the Schrödinger equation. This offers a unique platform for bridging condensed matter physics and quantum electrodynamics.

The most counter-intuitive behaviour exhibited by graphene is the anomalous quantum hall effect (minimum quantum conductivity in the limit of vanishing concentrations of charge carriers and strong suppression of quantum interference effects). Quantum Hall Effect (QHE) is usually observed at very low temperatures, typically below the boiling point of liquid helium (4K). Devices such as Hall-bars can be used to unravel the properties of graphene with the aid of e.g. a magnetic field. Under the influence of a magnetic field graphene shows a new type of quantum Hall effect [2]. The quantum Hall effect in general has been an intensive field of research since its discovery in 1980 by Klaus von Klitzing. Graphene has now enriched this field with a half-integer quantum Hall effect governed by massless relativistic particles [3]. It was even more surprising that the quantum Hall effect which is purely a quantum mechanical phenomena can be observed at the room temperature in this material.

Despite intense interest and continuing experimental success, widespread implementation of graphene has yet to occur. This is primarily due to the difficulty of reliably producing high quality samples, especially in any scalable fashion. So far, the original top-down approach of mechanical exfoliation has produced the highest quality samples, but the method is neither high throughput nor high-yield. However, for most applications, and for more elaborate experiments, we need large arrays of identical graphene devices, and have control over the size, shape, and location of each piece. Substrate-based growth of single layers by chemical vapor deposition (CVD), or the reduction of silicon carbide is the most promising technique to grow such big flakes of graphene [4]. It is a chemical process used to produce high-purity, high- performance solid materials. After nucleating a sheet, conditions must be carefully controlled to promote crystal growth without seeding additional second layers or forming grain boundaries [4]. The process is often used in the semiconductor industry to produce thin films.

1.2 Brief historical background

Theoretically, it was P.R.Wallace who first published a paper on graphene in 1947. He calculated the band structure of graphene and showed its unusual semi-metallic behavior [5]. The years thereafter graphene received a great deal of attention as a theoretical building block for more complex carbon structures such as graphite, and later carbon nanotubes and fullerenes. However the existence of graphene itself was ignored, as it would be unstable. From the studies, it was established that, in the standard harmonic approximation, the long-range order will be destroyed by the thermal fluctuations that would melt the 2D lattice [6] [7]. It was also presumed that during synthesis, the large perimeter-to-surface ratios at the graphene nucleation sites will favour the formation of other carbon allotropes like carbon nanotubes, fullerenes and graphite (see Fig. 1.1). With the discovery of a free standing graphene layer in 2004 all this perceptions were proved wrong. Its high crystal quality and the stability under ambient conditions attracted a great deal of attention. Such a two dimensional system with its unique electronic properties was never observed before. Moreover, its exceptional electronic properties promises a bright future in electronic industries.

1.2.1 Finding pin in a haystack

The most convinient way to obtain graphene flakes is through the micromechanical cleavage of HOPG (highly oriented pyrolitic graphite) crystals. The problem wth this technique is that the monolayer graphene flakes are extremely rare and hidden among thousands of thick (graphite) flakes. Even the modern techniques used for studying atomically thin materials are not good enough to locate graphene among the several micrometre-size crystallites. For example, scanning electron microscopy is inefficient in exactly determining the number of atomic layers present whereas the information obtained from the scanning-probe microscopy is insufficient to locate graphene precisely.

It was a very simple yet effective technique that resulted in the discovery of graphene. When placed on top of a Si/SiO_2 wafer, graphene gives a feeble interfernce-like contrast. This critical observation proved to be very effective for distinguishing graphene flakes from the bulk-graphite. The thickness of SiO_2 layer has to be carefully selected for locating graphene [1]. Currently, 300 nm thick SiO_2 on Si is widely used as the standard substrate. Even a 5% difference in SiO_2 thickness (315 nm instead of 300 nm) can make single-layer graphene completely invisible. Besides the knowledge of the SiO_2 thickness and the feeble contrast, it requires a great deal of patience and expertise to find graphene, as they are so thin that they can easily be overlooked. Recently, it was found that Raman microscopy is a quick and reliable method for determining the number of layers of graphene [8]. But the potential crystallites are still required to be scanned under optical microscope before its detection via. Raman spectroscopy.

1.3 Literature survey

This thesis is organized as follows: In the next chapter of the thesis, one can find an introduction to the properties of graphene. It gives a summary of the technique used for its synthesis, and a description of the common characterization methods that apply to graphene. The following chapter Sample Preparation Methods, and Equipments explains in detail the protocols involved in the synthesis of our samples (Chemical Vapor Deposition method) and in their characterization. It briefly describes the particular equipments used in our experiments (Scanning Electron Microscope, Evaporator, RIE (reactive ion etcher)). Further on, in Chapter 4, Results and Discussions are displayed regarding the technique used to fabricate graphene. With the obtained results we tried to conclude on the optimization of the parameteres required for graphene synthesis, on the samples characterization and on the progress made for their transfer. It summarizes the results of this work, showing the effect of sweeping gate voltage on the resistivity of graphene at room and low temperatues. Finally, all results and conclusions are summarized, and perspectives of future work necessary to carry out the low-temperature experiments are proposed.

Chapter 2

Properties of Graphene

2.1 The Linear Dispersion Relation

The dispersion relation of a material describes the interrelation of the energy with particle momentum along valence and conduction band. In conventional semiconductors, electrons are ascribed an effective mass m* that accounts for their transport under the influence of fields or carrier gradients. The electron energy depends quadratically on the momentum and can be written as

$$E=\hbar^2k^2/2m^* \quad (2.1)$$

(k is the electron wave vector).
Such a dispersion relation can be seen for example in graphite, where electron and

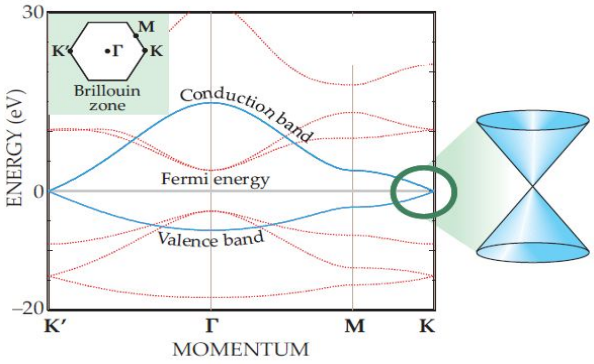

Figure 2.1: *Plot of the energy band structure of graphene along the MΓKM lines in the Brillouin zone. Valence and conduction bands just touch in a discrete point: the K-point. The energy-momentum dispersion relation becomes linear in the vicinity of this point (image taken from [9]).*

hole energy bands slightly overlap. When the numbers of layers is decreased, the overlap of the valence band and the conduction band becomes smaller and smaller

and disappears completely for just one layer [10]. In graphene the bands touch only in the K-point as shown in Fig.2.1. This results in a perfect electron-hole symmetry. The energy bands for graphene along the MΓKM lines in the Brillouin zone are shown in Fig 2.1. Near the K-point, the dispersion relation can be assumed to be linear. This model is best described by the following equation:

$$\mathrm{E} = \pm\hbar\vec{k}v_F \quad (2.2)$$

$\vec{k}$ is measured with respect to the K-point. By comparing this expression with the expression for the relativistic energy

$$\mathrm{E} = \pm(m^2c^4 + p^2c^2)^{\frac{1}{2}} \quad (2.3)$$

one recognizes that the dispersion relation of the electrons in graphene mimics a system of relativistic Dirac particles with a zero rest mass. The speed of light is replaced by the Fermi velocity $v_F = 10^6 m/s$ and $\hbar\vec{k} = \vec{p}$. The effective mass of the electrons and holes vanishes near the six corners of the two-dimensional hexagonal brillouin zone due to the lineraity of the E-k relation

$$\mathrm{E} = \pm(m^2c^4 + p^2c^2)^{\frac{1}{2}} \quad (2.4)$$

near these points [11]. The effective mass characterizes the behavior of an electron under the influence of applied forces at particular wave vectors. The disappearance of this parameter indicates that the electron velocity remains constant. Their transport properties becomes similar to those of massless Dirac particles like photons [3][12].

2.2 Electric Field Effect in Graphene

The electric field effect can be used to vary the charge carrier concentration in a graphene device. By changing the charge carrier concentration n the current can also be altered. An ambipolar electric field is used so that the charge carriers can be tuned continuously between electrons and holes. With this the charge carrier concentrations can reach values upto $n = 10^{13} cm^{-2}$ and the electron mobilities can exceed μ =15000 - 20000 $\mathrm{cm}^2 V^{-1} s^{-1}$ at room temperature [13]. It has been shown that the charge carrier concentration depends linearly on the gate voltage V_g , and μ does not significantly change as a function of temperature in a range of a few Kelvin up to room temperature [1][13].

The Fermi energy E_F level gets shifted with the change in the charge carrier concentration. The semimetal is transformed into a state with either completely

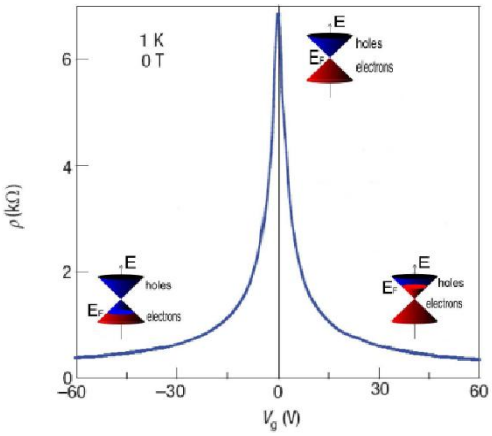

Figure 2.2: *Ambipolar electric field effect in graphene. This typical measurement was done at a temperature of 1 K and zero magnetic field (taken from [1]). The cones represent the low-energy spectrum, indicating the changes in the position of the Fermi energy E_F with increasing or decreasing gate voltage V_g. Negative V_g induces holes, positive V_g induces electrons.*

electrons or completely holes through a mixed state where electrons and holes are present (see Fig 2.2). At zero V_g the resistivity ρ has a maximum (Dirac point) at several $k\Omega$ and decreases to a few hundred Ω as the gate voltage is increased. In experiments, the position of this peak can often be found at larger voltages V_g. This shift is attributed to the unintentional doping of the device caused by impurities coming from the etchant solutions [14] [15].

2.3 Unconventional Quantum Hall Effect

In the ordinary Hall effect, a current I flowing along a conducting strip in the presence of a transverse magnetic field B causes a potential difference U_{xy} on the opposite sides of the electrical conductor. The ratio of the potential drop to the current flowing is called Hall resistance

$$\mathrm{R}_H = R_{xy} = U_{xy}/I = -B/I_{net} \quad (2.5)$$

In the classical Hall effect, the Hall resistance is directly proportional to the applied magnetic field and inversely proportional to the density n and charge e of the charge carriers (electrons) and the thickness t of the substrate. The longitudinal resistance of the bulk (3D) conductor along the flowing direction of the current can be written as

$$\mathrm{R}_{xx}^{3D} = \rho_{xx}^{3D} l/wt \quad (2.6)$$

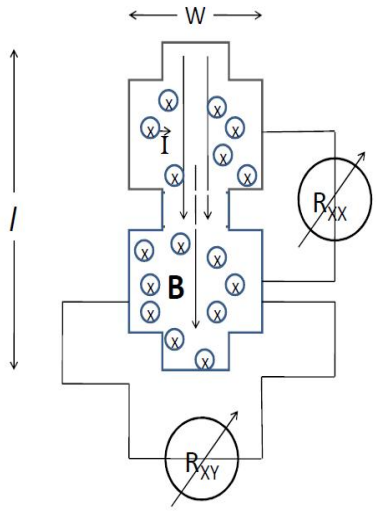

Figure 2.3: *If a current I is flowing through an electrical conductor and a perpendicular magnetic field B is applied a potential difference builds on the opposite sides of the substrate (represented by the black-white gradient). The size of the device is labeled by the width w and length l.*

with l being the length and w being the width of the substrate (see Fig 2.3). ρ_{xx}^{3D} is the material specific resistivity. In a two-dimensional electron gas (2DEG) at temperatures close to the absolute zero the Hall resistance becomes quantized and shows a plateau-like behavior. The longitudinal resistance in a 2DEG is defined as

$$\mathrm{R}_{xx}^{2D} = \rho_{xx}^{2D} l/w \quad (2.7)$$

The Hall resistivity that is directly proportional to the Hall resistance can take only discrete values of

$$\rho_{xy} = h/ie^2 \quad (2.8)$$

where h is the Planck constant, e the electric charge and i a positive integer.

The Quantum Hall Effect (QHE) observed in graphene is distinctively different from the conventional quantum Hall effects observed in several 2-D systems, because the quantization condition is shifted by a half-integer [16]. The electronic band structure of graphene near the K point forms the Dirac cone [17]. The electron and hole states are degenerate at this point. In the presence of a perpendicular magnetic field the charge particles of a conventional 2DEG occupy energy levels with discrete energy values called Landau levels (LL). However, the LLs in graphene is different from the LL appearing in conventional 2DEG devices due to linear dispersion relations. The most important characteristic of the LLs in grpahene is that they are not evenly spaced in energy. In presence of a magnetic field, the electronic spectrum

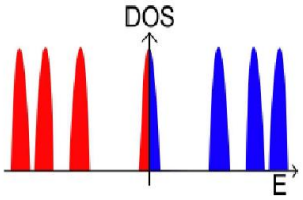

Figure 2.4: *Schematics of the Landau quantization in graphene: the sequence of Landau levels(LL) in the density of states (DOS) is described by* $E_N \propto \pm\sqrt{N}$ *for massless Dirac fermions. The LL at E=0 is independent of the magnetic field strength and therefore responsible for the unconventional QHE. The blue DOS refers to electron states and the red DOS to hole states(taken from [1]).*

of graphene shows the proportionality $E_N \propto \pm\sqrt{N}$ where N is the LL index and $\pm$ refers to electrons and holes (see fig 2.4). There is a LL at E=0 independent of the magnetic field strength. The unconventional half-integer QHE in graphene is attributed to the existence of this quantized level at zero E [18].

The formation of Landau levels under a perpendicular magnetic field in graphene

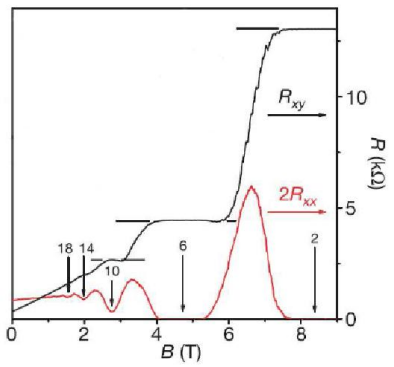

Figure 2.5: *The magnetoresistance* R_{xx} *(red) and the Hall resistance* R_{xy} *(black) are shown as a function of the magnetic field B at a temperature* $T = 30$ *mK and a fixed gate voltage* $V_g = 15$ *V.* R_{xy} *shows three plateaus at the filling factors* ν*=2,6 and 10 (graph taken from [15]).*

has been studied theoretically [1]. The Hall conductivity $\sigma_{xy} = \rho_{xy}^{-1}$ exhibits QHE plateaus when the Fermi energy E_F(tuned by varying the gate voltage V_g) falls between two LLs and exceeds by an amount of $\frac{4e^2}{h}$ when E_F crosses a LL. The double spin degeneracy and double valley degeneracy of the band structure introduces a factor 4 in the equation. The time-reversal invariance takes care of the particle-hole symmetry. The first plateau of σ_{xy} for electron and hole states is situated exactly at $\pm\frac{4e^2}{h}$. When E_F crosses the next electron(hole) LL, the Hall conductivity increases by an amount $\frac{4e^2}{h}$. This leads to the following quantization condition:

$\sigma_{xy}^N = \frac{1}{\rho_{xy}^N} = 4(N + \frac{1}{2})\frac{e^2}{h}$ (2.9)

From Fig. 2.5, it is evident that the conductivity σ_{xy}^N shows a step like half-integer quantization at a constant magnetic field B and a constant temperature T of a few Kelvin. At the same time ρ_{xy}^N shows peaks when σ_{xy}^N jumps to the next plateau.

Fig. 2.5 shows the magnetoresistance R_{xx} and the Hall resistance R_{xy} as a function of the magnetic field B at a fixed gate voltage V_g. R_{xy} shows a step like behavior with plateaus at high magnetic fields where R_{xx} is vanishing. The three plateaus are shown with resistivity values $\rho_{xy}^0 = h/2e^2$, $\rho_{xy}^1 = h/6e^2$ and $\rho_{xy}^2 = h/10e^2$. The values ν=2, 6, 10 or in general ν=4(N + 1) are called filling factors.

2.4 The focus of my work

Large-area growth of graphene is required for the development and large-scale production of electronic devices. Recently, chemical vapor deposition (CVD) of hydrocarbons has proved to be the most promising of all techniques for growing large-area graphene films on metal substrates such as Nickel (Ni) and Copper (Cu). CVD is a chemical process where a wafer (substrate) is exposed to one or more volatile precursors, which react and/or decompose on the substrate surface to produce the desired deposit. The proposed mechanism for the CVD growth of graphene is by Carbon atom segregation or precipitation process over Ni sucbstrate and by surface adsorption process for growth over Cu substrate [19].

Several groups have already demonstrated that few layer graphene can be produced by the CVD growth on Ni and Cu. Here we used Cu foils as the substrate because of the low solubility of Carbon atoms on Copper. The growth of graphene on Cu is believed to be surface-mediating and self-limiting. Ni, on the contrary have not yeilded uniform graphene layers, i.e., they have a wide variation in growth thickness(from monolayer to many layers) over the metal surface. Fig. 2.6 shows the SEM image of the graphene grown on Cu foils. A thick layer (290 nm) of PMMA is deposited on graphene and the Cu foils were etched out from beneath. The resulting graphene film is transferred onto a Si substrate with 300 nm of SiO_2 on top of it. Fig 2.7 shows the optical image of the graphene transferred on a SiO_2/Si substrate. The surface of the transferred graphene is relatively uniform with the exception of wrinkles. These wrinkles are believed to be formed during cool-down of the temperature of the furnace. The wrinkles are a result of the different coefficient of thermal expansion between graphene/graphite and the underlying metal substrate [19].

We grew large-area graphene films of the order of centimeters on Cu substrates. We used methane (CH_4) and forming gas (hydrogen and nitrogen) as the precursor gases and the copper foils (25 μm thick) are used as the substrate. The generally believed mechanism for the growth of graphene is that at high temperature CH_4 gets decomposed into carbon (C) and hydrogen (H) atoms. The carbon atoms get adsorbed over the Cu foils and as the system cools down, these atoms come over the surface and segregate to form graphene layer. This transformation into a more crys-

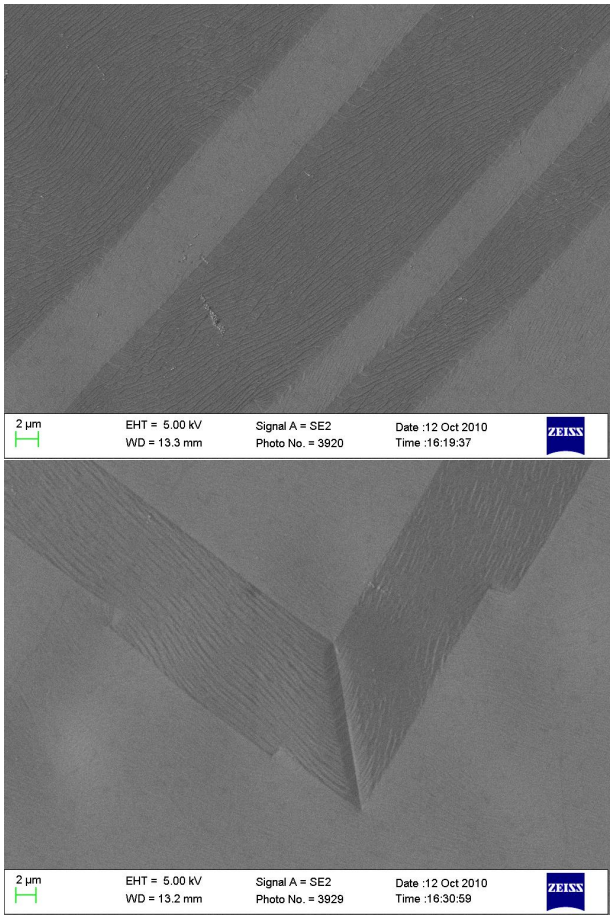

Figure 2.6: *Graphene grown on Copper foils at* T=1025 °C, *Pressure=15 mbar, growth period=8 minutes.*

talline form from an amorphous state requires thermally assisted kinetic process involving nucleation and growth. Copper because of it's catalytic nature provides such assistance. Graphene is believed to grow over step edges and traces of crystalline surface, so annealing of copper was done at 1025 °C to ensure a smooth crystalline surface for graphene growth. The films so produced are found to be predominantly single-layer graphene, with a small percentage (less than 5%) of the area having few layers, and are continuous across Cu surface steps and grain boundaries. The low solubility of carbon in Cu appears to help make this growth process self-limiting.

The so-obtained graphene is covered with a thick layer of EL9 resist ($\sim$ 300 nm) to make the handling of otherwise invisible graphene easier. The Cu is etched out using the ferric chloride/sodium persulfate solution. Normally, the etchant leaves a lot of residue on graphene after etching out the Cu foils, sodium persulfate is found to show better results in this regard. The floating flake of PMMA + graphene is rinsed 5-6 times in water before carefully transferring it over Si/SiO_2 substrate. The resist is allowed to dry by itself so that the water gets enough time to wick out from the corners. It was observed that the drying period was very crictical because keeping it

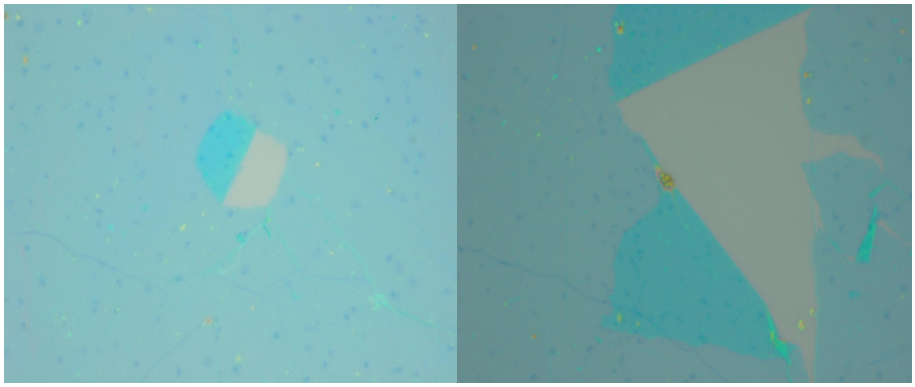

Figure 2.7: *Graphene transferred to the SiO_2/Si substrate.The image size is 800 μm^2*

for long makes it difficult to remove the resist completely and shorter drying period does not provide good adhesion between the graphene and Si substrate. We also developed the graphene film transfer processes to SiO_2 substrates, since the graphene flakes are very fragile and crumple under tension. After the transfer and drying the resist (EL9) layer can be washed out in acetone and rinsed with IPA (Iso-propyl alcohol) and we are finally left with graphene or Si/SiO_2 substrate. The field-effect transistors (FETs) were fabricated on Si/SiO_2 substrates using the electron-beam lithography. Electron Beam Lithography (EBL) refers to a lithographic process that uses a focused beam of electrons to form the circuit patterns needed for material deposition on (or removal from) the wafer, in contrast with optical lithography which uses light for the same purpose. Electron lithography uses the electrons of 10-50 keV which has a shorter wavength that offers higher resolution. The details of principle and working of the e-beam lithography techinique is discussed in the next chapter. The electronic meaurements on the devices showed electron mobilities as high as 50 $cm^2V^{-1}s^{-1}$ at room temperature and 7000 $cm^2V^{-1}s^{-1}$ at low temperature (1.4 K).

Chapter 3

Sample preparation methods and Equipments

The aim of this chapter is to describe the necessary techniques to grow graphene by the CVD method, transferring it to the Si/SiO_2 substrate and to fabricate devices on it using e-beam lithography. Finally there is an overview on all the equipments (e.g. Scanning electron microscope, Evaporator, Reactive ion etcher(RIE)) used during the fabrication process.

3.1 Chemical vapor deposition

The details of the preparation technique are as follows:

i. The 25 μm thick Copper foils were cut 1 cm^2 and flattened by stamping it between two glass slides.

ii. The foils were cleaned in the following sequence with Acetone (30 Sec), Water (1 minute), Acetic Acid (10 minutes), Water (1 minute), Acetone (30 sec) and IPA (30 Sec). Then, we gently dry the Cu foils using a low flow nitrogen.

iii. These foils were put inside the furnace shown in Fig 3.1 using a quartz boat. The furnace had three consecutive heating zones. All the three zones were kept at 1025 °C and a low pressure (1.2e-2 mbar) is achieved using a vacuum pump.

iv. A flow of 20 sccm (standard cubic centimetre per minute) of forming gas is blown initially for 30 minutes to anneal the Cu surface and to remove any oxygen content. This brings down the pressure to around 1.6e-1 mbar.

v. We used an MKS mass flow controller to maintain the flow of methane and forming gas inside the furnace. A 100 sccm flow of methane gas is started along with the hydrogen flow. The pressure is maintained at 15 mbar.

vi. The growth period of graphene starts as soon as the methane is blown in the furnace and terminates when the furnace starts to cool down. The cooling

Figure 3.1: *The experimental set up for the CVD growth of graphene . The furnace, pressure gauge, vacuum pump with butterfly valve, MKS mass flow controller (in clockwise order from the left top).*

rate of the furnace is a crucial factor for the monolayer growth of graphene [3]. Usually inbuilt water circulation is there to cool down the furnace. But, the rate of cooling was not sufficient, so we modified the set-up and attached an exhaust at one end of the furnace so that the cooler air can come from the other open end that improved the cooling rate. The growth period has been varied from 8 minutes-25 minutes to check the time dependence of thickness of graphene layers.

vii. The furnace was allowed to cool down to the room temperature. Any volatile by-products produced were removed by flowing argon gas through the reaction chamber for 5 minutes. High quality crystalline growth of graphene have been reported by this technique.

viii. The samples were taken out of furnace.

ix. A 310 nm thick layer of EL9 resist is coated over it. The resist is coated by spinning it over the substrate at 3200 rpm for 45 sec and baking at 180 °C for 7 minutes.

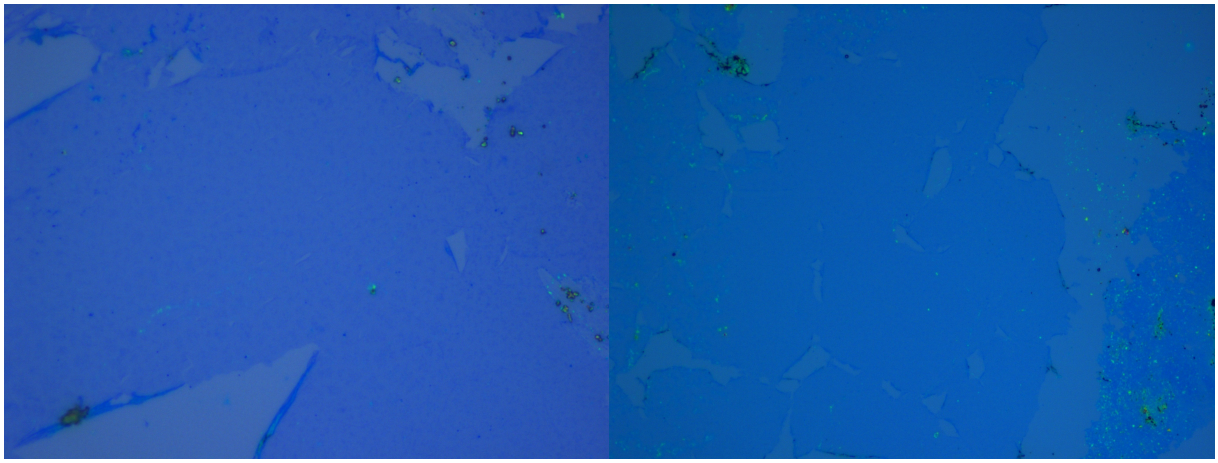

Figure 3.2: *Graphene transferred over Si/SiO_2 subtrate. The dimension of the image is a)200 μm^2 b)800 μm^2*

x. The Cu from the resist-coated foils were etched out using 0.25 g/ml solution of Sodium persulfate.

xi. The Cu was etched out and a transparent layer of EL9 + graphene floats on the surface of the solution. This was cleaned with DI water for $\sim$ 6 times and transferred over the Si/SiO_2 substrate.

xii. The sample was allowed to dry so that the water gets enough time to wick out from the edges. The drying period was optimized to be around 2 hours because drying for shorter periods does not allow good adhesion between the graphene and Si substrate whereas drying for long makes the removal of resist layer very difficult.

xiii. The substrate is then cleaned with acetone (for 1.5 hours) to dissolve the EL9 resist layer and rinsed with IPA (to prevent acetone residues). The so-obtained graphene over Si/SiO_2 substrate is shown in Figure 3.2.

xiv. Relatively cleaner areas of graphene were determined from the optical microscope and the images were imported to write a Computer Aided Design (CAD) on it.

xv. The graphene over Si/SiO_2 substrate was coated with EL9 (310 nm thick) and PMMA 950 A2 (95 nm thick) resist for e-beam lithography.

xvi. The hall-bar devices were fabricated over this graphene using e-beam lithography. An optical image of a CAD written over the sample is shown in Fig. 3.3.

xvii. The CAD was written on the device and then developed using MIBK (90 sec) and IPA (60 sec) respectively. IPA was blown out of the substrate by using low nitrogen flow.

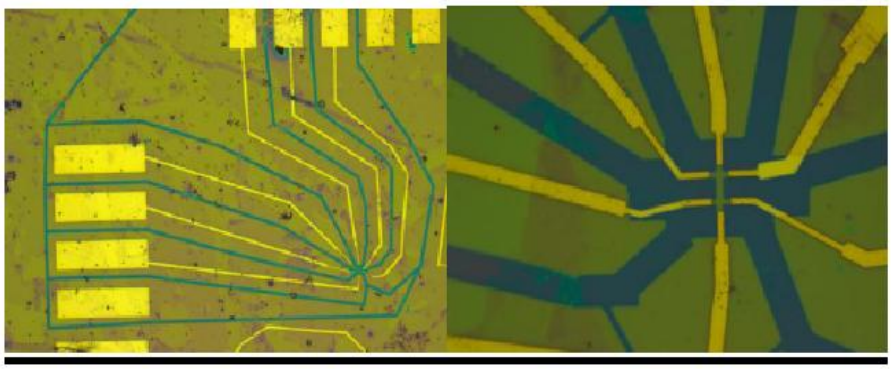

Figure 3.3: *a) A Hall-bar device fabricated over graphene (5000 μm^2). b) The zoomed image of the device is 200 μm^2.*

xviii. 10 nm Chromium and 60 nm of gold was deposited on the trenches (created by the e-beam lithography) by thermal evaporation. This acts as the electrodes during the measurement. The unnecessary gold deposited all over the substrate was lifted off by keeping in acetone for 30 minutes.

xix. The graphene was distributed uniformly all over the substrate. So, to prevent the electrodes from being shorted, another CAD was designed as the mask so as to protect the deivce area when the rest of the graphene will be etched out. The mask was also written by e-beam lithography.

xx. We used a negative resist HSQ (Hydrogen silsesquioxane) to write the mask. The advantage with negative resist is that the region that is exposed to the e-beam becomes hard. While developing the resist, the unexposed portion gets washed away.

xxi. This exposes the graphene in the unmasked region to be etched out by oxygen plasma in RIE (Reactive Ion Etcher).(Graphene etching recipe⇒ Power=50 W, time=4 min. 30 sec.). The masked area protects the graphene on the device.

xxii. The resist from the masked region was removed by keeping in buffered HF (for 5 minutes).

xxiii. The sample was washed in acetone and was mounted on the chip carrier. The electrodes of the device were wire-bonded with the contacts of the chip carrier.

xxiv. The devices on these standard chip carriers can be inserted in the cryostat for low temperature measurements.

3.2 Equipments

3.2.1 E-beam lithography

Electron-beam lithography uses electrons instead of photons to expose a resist. Since, electrons have a much smaller wavelength than the light used in photolithography, it has a much higher intrinsic resolution. The electron beam can be focused onto a substrate directly and can be controlled so that it only exposes those areas which ought to be exposed. Conventional electron-beam lithography is done using an SEM (see Fig 3.5). SEM can give electrons energies up to about 30 keV, and uses an electron beam with a diameter of a few nanometers. The high energy electrons were made to strike a sensitive material called resist that is physically or chemically modified by the exposure of the electron beam. The energy deposited during the exposure creates a latent image that is materialized during chemical development. For positive resist, the development creates trenches wherever it is exposed whereas the inverse occurs for the negative resist (see Fig.3.4).

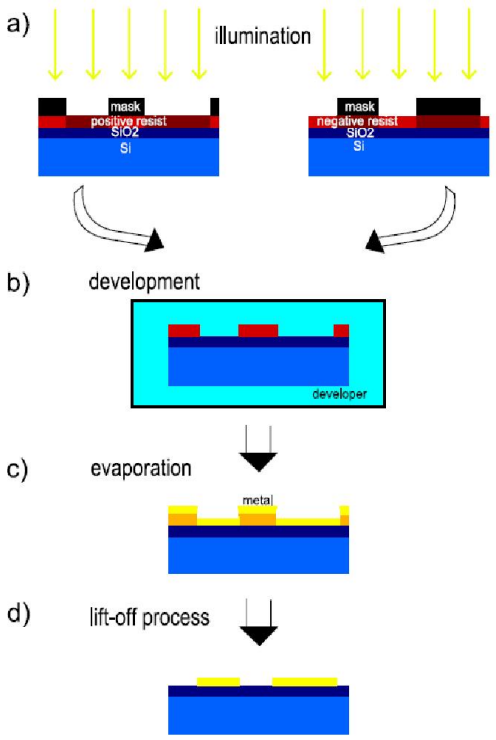

Figure 3.4: *a) Photoresist is spun on a silicon wafer with a SiO_2 layer. After putting the mask with the desired structure on the sample it can be exposed by light. b) After developing the sample c) Gold is evaporated on the whole sample. d) The lift-off process in acetone removes the remaining photoresist.*

Operation principle

The SEM that we used has a LaB_6 field emmision electron source. LaB_6 is a thermal filament but since its work function is lower than the tugsten filament, it is more efficient. In a field emission source, a strong electric field is applied very close to the filament. The high size and proximity effect of the electric field causes the electrons to tunnel out of the electron reservior in the filament. The electron beam is focused by one or two condenser lenses to a spot about 0.4 nm to 5 nm in diameter. The beam passes through pairs of scanning coils or pairs of deflector plates in the electron column, typically in the final lens, which deflect the beam in the x and y axes so that it scans in a raster fashion over a rectangular area of the sample surface. The energy exchange between the electron beam and the sample results in the reflection of high-energy electrons by elastic scattering, emission of secondary electrons by inelastic scattering and the emission of electromagnetic radiation, each of which can be detected by specialized detectors. Electronic amplifiers of various types are used to amplify the signals which are displayed as variations in brightness on a cathode ray tube. The raster scanning of the cathode ray tube (CRT) display is synchronised with that of the beam on the specimen in the microscope, and the resulting image is therefore a distribution map of the intensity of the signal being emitted from the scanned area of the specimen.

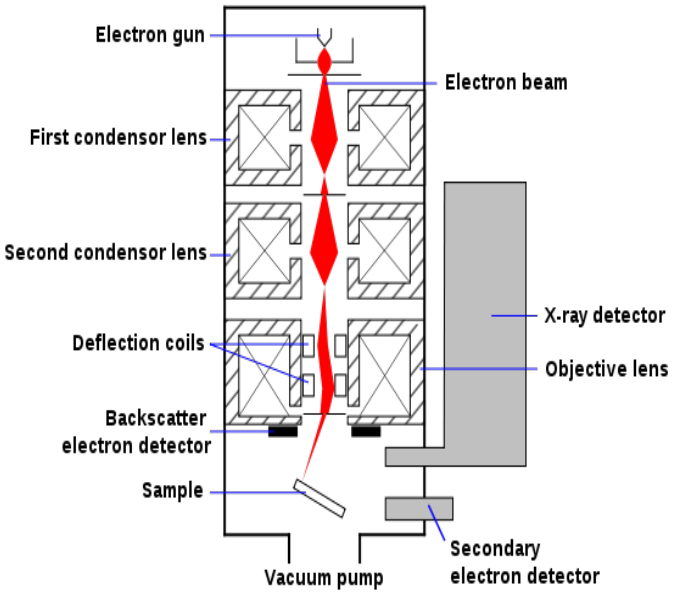

Figure 3.5: *A schematic diagram of a Scanning Electron Microscope(from [20]).*

Electron beam lithography is carried out on electron-sensitive resist materials such as the polymer, PMMA. Solutions of the resist are spin-coated onto a sample and baked to leave a hardened thin-film on the surface of sample. The EBL system is then used to move a focused electron beam across the sample to selectively expose a pattern in the resist previously designed with the system's in-built Computer Aided Design (CAD) tools. Exposure of a positive resist such as PMMA to electrons causes

fragmentation of the polymer chain into smaller molecular units in a process known as chain-scission. A suitable developer solution can then be used to selectively dissolve the fragmented polymer chains in the exposed areas of resist, whereas the unexposed resist remains insoluble in the developer solution. The process therefore leaves a patterned resist mask on the sample that can be used for further processing on the sample.

3.2.2 Gold deposition by thermal evaporation

In thermal evaporation technique a solid material (pure metal, eutectic or compound) is vaporised by heating it to sufficiently high temperatures and recondensing it onto a cooler substrate to form a thin film. The heating of the metal is carried out by passing a large current through a filament container which has a finite electrical resistance.

Once the metal is evaporated, its vapour undergoes collisions with the surrounding gas molecules inside the evaporation chamber. As a result a fraction is scattered within a given distance during their transfer through the ambient gas. For most of the evaporated species pressure lower than 1e-6 torr are necessary to ensure a straight line path for substrate-to-source distance of approximately 10 to 50 cm in a vacuum chamber. Good vacuum is also a pre-requisite for producing contamination free deposits. These systems have a crystal monitor which is connected to film thickness monitor to control the amount of metal deposit. We deposited 10 nm of chromium and 60 nm of gold on the sustrate by this method. Chromium is deposited to provide better adhesion of gold with the substrate.

3.2.3 RIE etching

The CVD graphene obtained contains a lot of impurities in the form of left over residues of PMMA and sodium persulfate. In order to do the electronic measurements in it, we have to selcet a relatively cleaner portion so as to minimize the effect of impurities. A hall-bar of approximately 80 μm^2 was designed to study the electronic properties. The rest of the graphene has to be etched out to prevent the shorting of electrodes.

In RIE, the substrate is placed inside a reactor where several gases can be introduced. A RF power source is used to break the molecules of the gas into ions that struck a plasma in the gas mixture. The surface of the material comes in contact with these accelerated ions and forms another gaseous material. This way the exposed metal surface is etched chemically. The physical etching in RIE is similar to the sputtering deposition process. In this process the high energy ions can knock atoms out of the substrate without a chemical reaction. There are a number of parametres that needs to be optimized to develop a dry etch processes that balances chemical and physical etching. The chemical etching is isotropic whereas the physical etching is anisotropic, so it is possible to influence the anisotropy of etching by changing the paramenters. A schematic of a typical reactive ion etching system is shown in Fig 3.6.

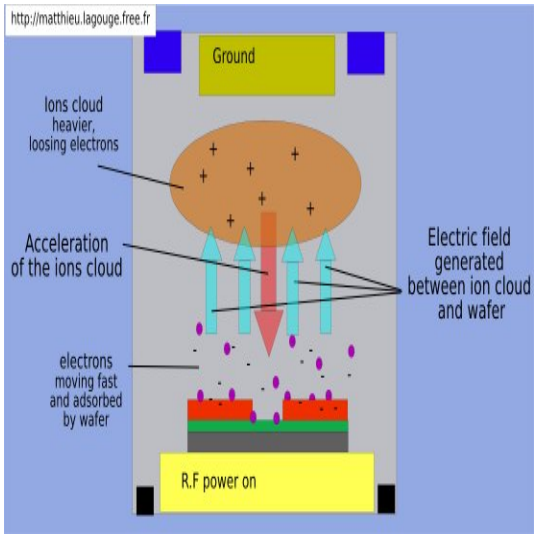

Figure 3.6: *A schematic diagram of a RIE(image taken from [21])*

We first did etching tests in order to find the optimal etching parameters. To etch a single or few layer graphene flake the sample was kept in oxygen plasma R_f power 50 W for 4 minute 30 seconds. This etching can also be used to etch thicker layers that can cause shorting between two electrodes. Shorting between the contacts can happen if there are other big flakes in the environment of the flake one wants to contact. However, if thicker layers has to be etched one has to take into consideration that the PMMA/HSQ is also etched by the oxygen plasma at a rate of 70 nm/minute. For this reason the used PMMA/HSQ should have adequate thickness. Another important point to be kept in consideration was that long etching period could bake the sample which makes it impossible to remove from the acetone. A chemial fluid was used to stick the substrate which provides the local cooling to the substrate and hence prevents the baking of the resist.

Chapter 4

Results

In this chapter we present the result of the measurements done on the devices and its interpretation. The graphene synthesized from the Chemical Vapor Deposition method is shown in Fig 3.2. From the optical image it was visible that it had a lot of impurities. The sample was analyzed in SEM/EDAX to qualitatively determine the impurities. The result is shown in Fig.4.1

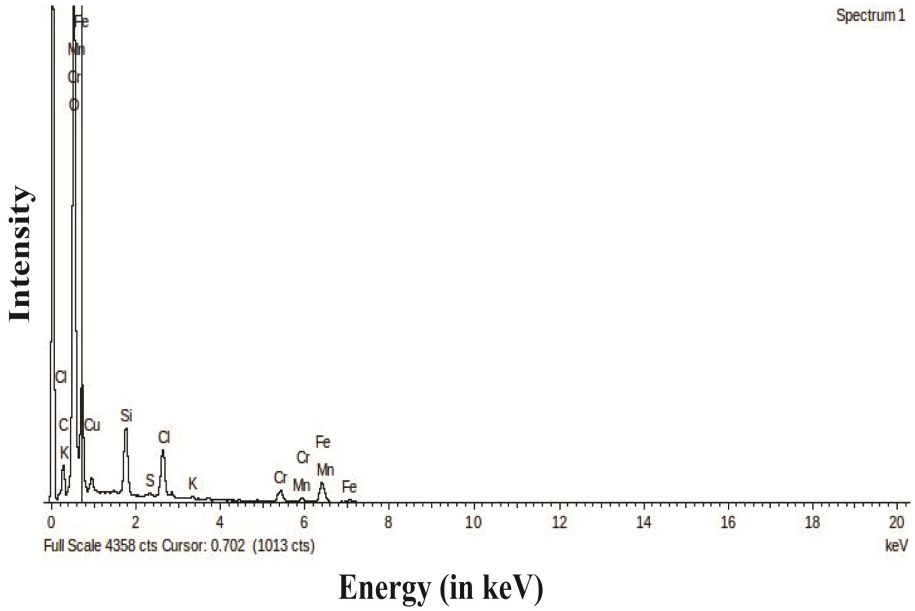

Figure 4.1: *EDAX of the first graphene sample produced*

It shows the presence of Fe, Ni, Cr, Mn and Cl atoms. The only possible source for these impurities could be Ferric Chloride solution which was used to etch Cu. It was later replaced by sodium persulfate (0.25 g/ml) which gave better results. The devices were fabricated by using e-beam lithography and we did some room temperature measurements.

We fabricated several hall-bar devices to measure its electronic properties. The optical image of the device is shown in Fig.4.2.

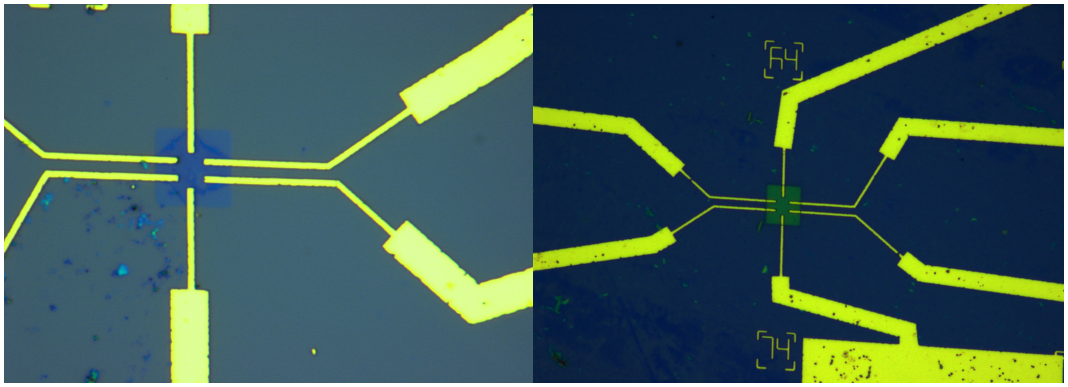

Figure 4.2: *Comparison of the device after (Image size : 200 μm^2) and before (Image size : 800 μm^2) the etching of the negative resist HSQ*

4.1 Room temperature measurements

4.1.1 Raman test

Raman spectra can very accurately determine the single layer, bilayers, and few layers graphene since it uniquely captures the electronic structure of graphene. Thus it provides an unambiguous, high-throughput, nondestructive identification of graphene layers[22]. The two most important features of graphene electronic structure are the presence of a G peak at 1500 cm^{-1} and a band at 2700 cm^{-1}.

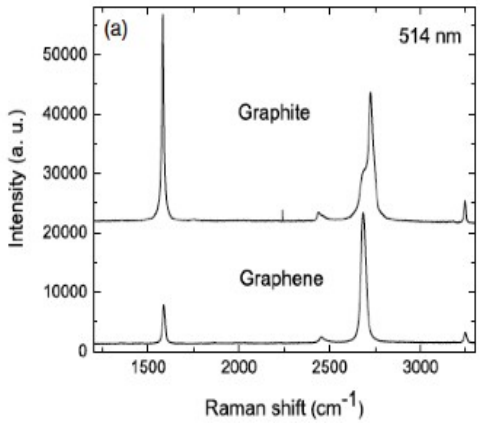

Figure 4.3: *Comparison of Raman spectra at 514 nm for bulk graphite and graphene. They are scaled to have similar height of the 2D peak at 2700 cm^{-1} (from [22]).*

The band (2D peak) is the second order of zone-boundary phonons. Since zone-boundary phonons do not satisfy the Raman fundamental selection rule, they are not seen in first order Raman spectra of defect-free graphite. Fig 4.3 compares the 514 nm Raman spectra of graphite and graphene. In graphene the 2D peak is roughly 4 times more intense than the G peak. The 514 nm Raman spectra of our samples yeilded the following results as shown in Fig 4.4 and Fig 4.5. Fig. 4.4

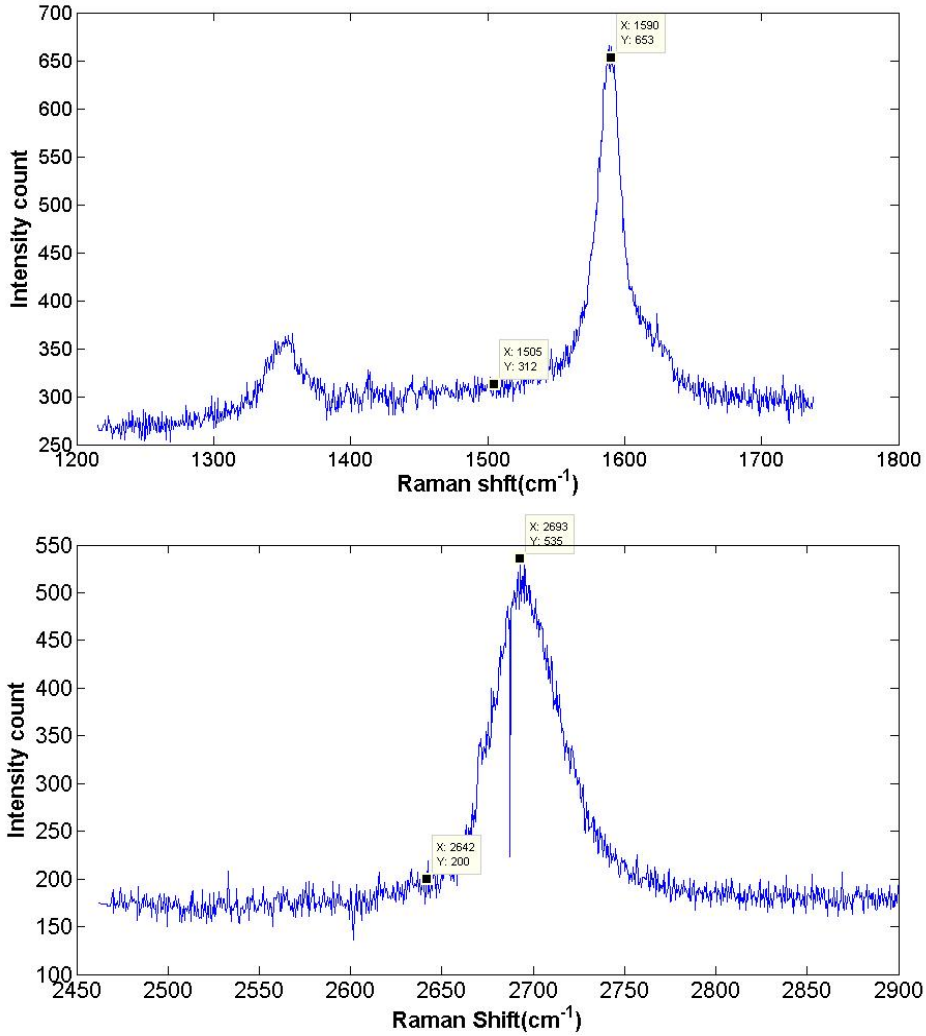

Figure 4.4: *The raman spectra of the graphene device, a) G peak at 1590 cm^{-1} b) 2D peak at 2700 cm^{-1}*

shows the raman spectra of the graphene where we fabricated the Hall-bar devices whereas Fig. 4.5 shows the raman spectra of the graphene sample near the edges of the Si/SiO_2 substrate. From Fig. 4.4 it is clear that the 2D peak was comparable to the G peak and the ratio of 2D and G peak was found to be $\frac{2D}{G} = \frac{335}{341} = 0.98 \simeq 1$. Although the 2D peak was not very sharp but this could be because of the fact that our samples were not absolutely clean. The $\frac{2D}{G} = \frac{212}{563.5} = 0.376$ for the region near the edges. The peak ratio was similar to the graphite bulk. This was expected because near the edges mostly the flakes crumples during the transfer to the substrate, thus forming a lump of graphene flakes.

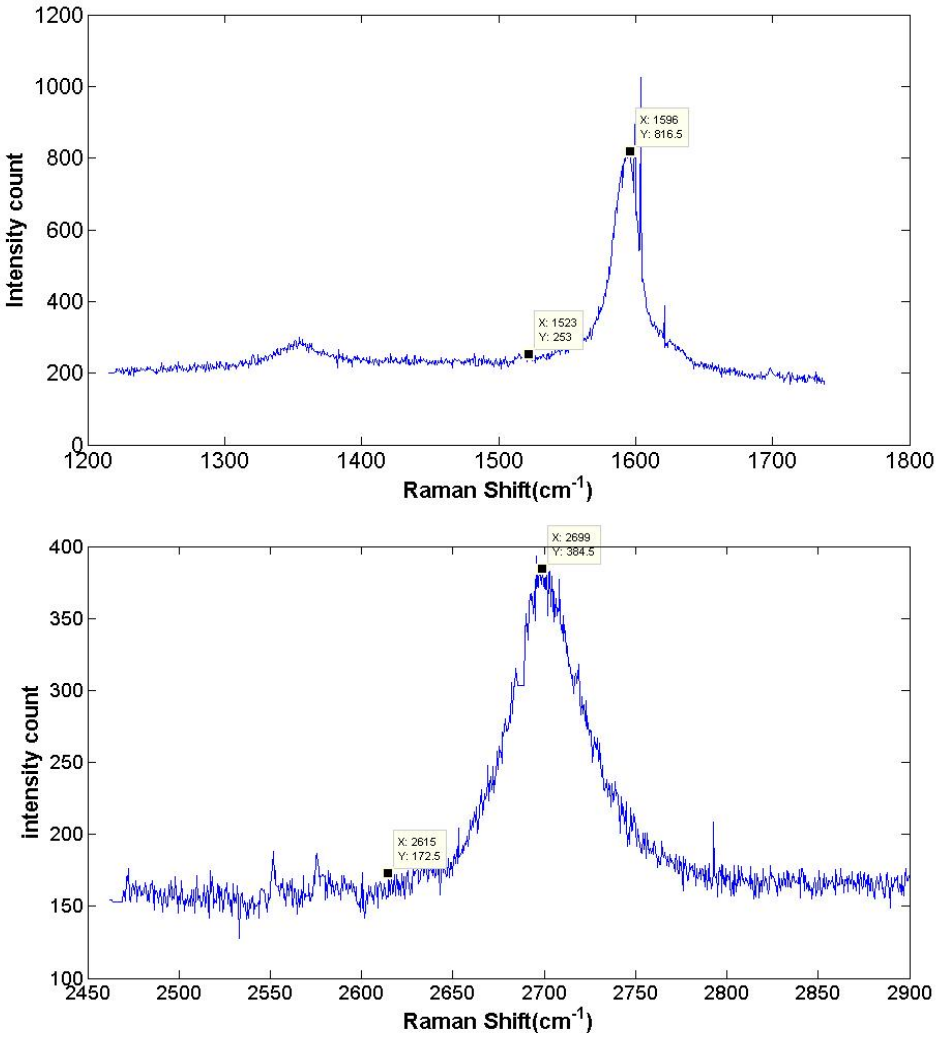

Figure 4.5: *The raman spectra for the region away from the device (near the edges) a) G peak at 1590 cm^{-1} b) 2D peak at 2700 cm^{-1}*

4.1.2 Gate Sweep effect

The electric field effect in graphene was described in chapter 2.1. Electric field effect can be used to dope graphene either with electrons or holes, resulting in a minimum conductivity at the charge neutrality point. To measure the gating effect we used the degenerately doped Si of the wafer as a back gate. The back gate was connected by putting silver paint at the bottom. The 300 nm of insulating SiO_2 layer works as a gate dielectric. We swept the gate voltage from -20 to +20 V at room temperature and the conductance of the device was measured. Fig. 4.6 represents the low-bias conductance G as a function of a backgate bias V_g applied to the Si substrate.

The conductance decreased continuously as we increased the gate voltage V_g, which indicates that the conductance minimum is beyond the voltage range. The $\triangle$G/G ratio was measured to be ~ 0.175. We did not observed the Dirac peak at

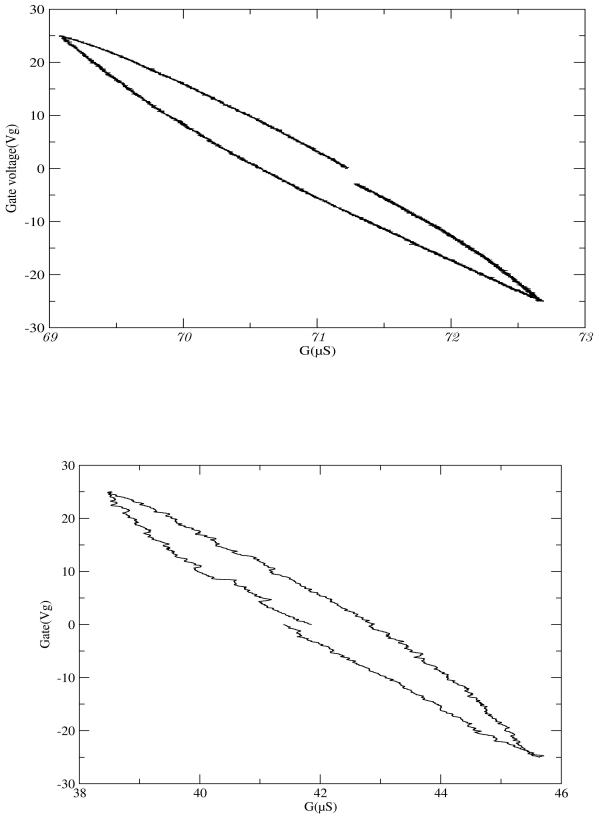

Figure 4.6: *A plot of Conductance (G) vs Back gate voltage (V_g) at room temperature*

room temperature. Ideally, the minimum conductivity should be at zero gate bias, however the plot shows a shift away from the Dirac zero point. Most likely the cause for this shift is the presence of impurities, residues left from the Cu etching solution(sodium persulfate) or HSQ etchant(HF). For this sample, the electron mobility was calculated as 50 $cm^2V^{-1}s^{-1}$.

4.2 Low temperature measurements

The sample was cooled to 1.4 K and the gate voltage was swept from -20 V to 50 V. A magnetic field perpendicular to the device was applied and it was varied from 0 to 14 T in the steps of 0.2 T. The bias gate voltage was swept from -20 to 50 V for each value of the magnetic field. As the magnetic field increased to 9 T the dirac peak appeared. The dirac peak was shifted by 32 V on the positive bias. The mobility of the device shown in Fig.4.8 was calculated to be 7000 $cm^2V^{-1}s^{-1}$. The calculation is shown in the appendix.

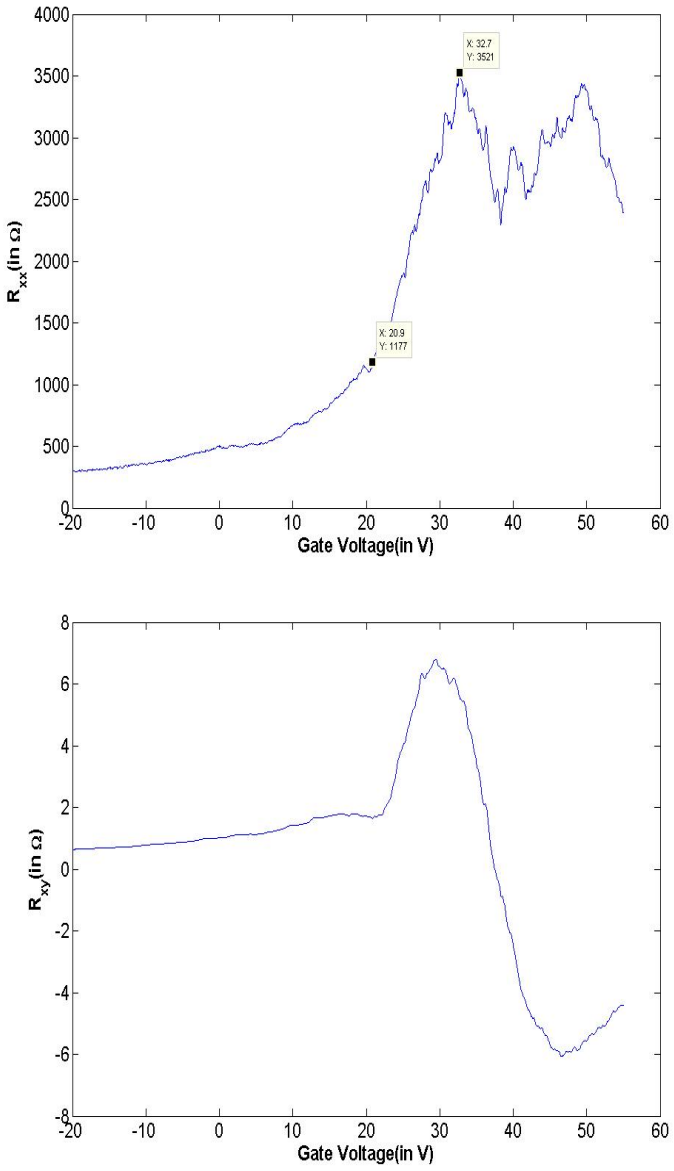

Figure 4.7: *A line plot of longitudinal resistance(R_{xx}) Vs V_g and transverse resistance(R_{xy}) Vs V_g for monolayer graphene device at 1.4 K and 9.8 T*

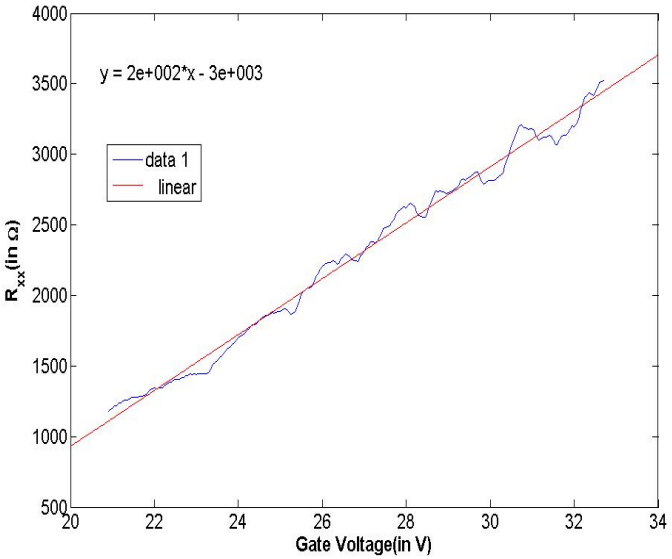

Figure 4.8: *A slope of R_{xx} Vs V_g*

Ideally, the presence of a dirac peak confirms the the presence of monolayer graphene. The low temperature measurements of the magnetoresistance of our samples at 1.4 K yeilded the results as shown in Fig. 4.7. In the graph we can see three dirac peaks at 32 V, 40 V and 50 V respectively. The multiple dirac peaks may be a result of the charge inhomogenity of our samples. The non-uniform distribution of charge carriers creates multiple neutrality points which gives rise to multiple dirac peaks.

Chapter 5

Summary

Graphene is one of the most interesting materials in mesoscopic physics today. The unusual properties of the charge carriers and exceptional electronic quality promises a bright future in electronics industry that may not be attainable by conventional silicon based devices. Till date the highest quality graphene samples were produced by mechanical exfoliation but intensive research is going on to produce large scale graphene. In summary, we have developed the CVD method to grow and transfer high-quality graphene films on a large scale. Very exciting results have been reported on the CVD grown graphene. We were able to produce graphene flakes in our laboratory with carrier mobilities of around 7000 $cm^2V^{-1}s^{-1}$. These mobilities are comparable to the mobilities of the samples produced by the Geim group and the Ruoff group. A conclusion of the electric field effect measurement is that the charge neutrality point is shifted to a very large positive gate voltage. This shift indicates that there is a heavy doping of the sample due to transferred charges during the device-fabrication process. The relative low mobility observed at the room temperature in this sample could be attributed to the unintentional chemical doping from sodium persulfate and HF. The doped ions have high kinetic energy at room temperature to overcome the effect of the charge induced by sweeping the gate voltage. The high mobility measured at low temperature may be due to the fact that as the sample cools down to 1.4 K, the ions get frozen (lose their kinetic energy) and we could observe the effect of the biased gate. Also, the current has been passed through our samples for very long time during the low temperature measurements, so, the current-induced cleaning of graphene could also improve the mobility [23]. In future we will concentrate on fabricating high quality devices from CVD with higher mobilities. It will be interesting to probe the non-equilibrium QHE with these devices.

References

[1] A. K. Geim, K. S. Novoselov, The rise of graphene, Nature Materials **6** (2007) 183–191.

[2] Z. Jiang, Y. Zhang, Y. W. Tan, H. L. Stormer, P. Kim, Quantum hall effect in graphene, Solid State Communications **143** (2007) 14–19.

[3] N. K. S. et al., Two-dimensional gas of massless dirac fermions in graphene, Nature **438** (2005) 197–200.

[4] M. J. Allen, V. C. Tung, R. B. Kaner, Honeycomb carbon- a review of graphene, Chemical Review **110** (2010) 132–145.

[5] P. R. Wallace, The band theory of graphite., Phys. Rev. **71** (1947) 622–634.

[6] Peierls, R. E. Quelques, Proprietes typiques des corpses solides, Ann. I. H. Poincare **5** (1935) 177–222.

[7] Landau, L. D. Zur, Theorie der phasenumwandlungen ii., Phys. Z. Sowjetunion **11** (1937) 26–35.

[8] Y. ying Wang, Z. hua Ni, T. Yu, Z. X. Shen, H. min Wang, Y. hong Wu, W. Chen, A. T. S. Wee, Raman studies of monolayer graphene: The substrate effect, J. Phys. Chem. C **112** (2008) 10637–10640.

[9] A. K. Geim, A. H. MacDonald, Graphene: Exploring carbon flatland, Physics Today **60** (2007) 35–41.

[10] B. Partoens, From graphene to graphite: Electronic structure around the k-point, Physical Review, B **74** (2006) 075404–1–075404–11.

[11] J.-C. Charlier, E. P.C., J. Zhu, A. Ferrari, G. D. Eds. A. Jorio, M. Dresselhaus., Carbon Nanotubes: Advanced Topics in the Synthesis, Structure, Properties and Applications, Springer-Verlag Berlin/Heidelberg, 2008, Ch. Electron and Phonon Properties of Graphene: Their Relationship with Carbon Nanotubes.

[12] M. Wilson, Electrons in atomically thin carbon sheets behave like massless particles, Physics Today **71** (2006) 21–23.

[13] K. Novoselov, Room-temperature electric field effect and carrier-type inversion in graphene films, arXiv:cond-mat/0410631v1.

[14] Novoselov, K. S. et al., Electric field effect in atomically thin carbon films, Science **306** (2004) 666–669.

[15] Z. Y., T. J.W., S. H.L., K. Novoselov, Experimental observation of the quantum hall effect and berry's phase in graphene, Nature **438** (2005) 201–204.

[16] T. Heinzel, Mesoscopic electronics in solid state nanostructures, Wiley-VCH.

[17] K. Novoselov, Room-temperature quantum hall effect in graphene, Science **315** (2007) 1379.

[18] Y. Zheng, Hall conductivity of a two-dimensional graphite system, Physical Review B **65** (2002) 245420–2–245420–11.

[19] X. L. et al., Large-area synthesis of high-quality and uniform graphene films on copper foils, Science **324** (2009) 1312–1314.

[20] http://en.wikipedia.org/wiki/FileSchemaMEB.

[21] http://matthieu.lagouge.free.fr/microtechnology/dryetch.html.

[22] A. C. Ferrari, J. C. Meyer, V. Scardaci, C. Casiraghi, S. Piscanec, D. Jiang, K. S. Novoselov, S.Roth, A. K. Geim, Raman spectrum of graphene and graphene layers, Phys. Rev. Lett. **97** (2006) 187401.

[23] Moser, Barriero, Batchtold, Current induced cleaning of graphene, Applied Physics Letters **91** (2007) 163513.

Appendix A

Mobility calculation

The mobility of a hall-bar device is given by

$\mu = L^2 m/C$ (A.1)

$\mu \rightarrow$ mobility of the carriers
L $\rightarrow$ distance between source drain = 6 μm
C $\rightarrow$ parallel plate capacitance
m $\rightarrow$ slope of the conductance vs Gate voltage = 200 μS/V
C = Aε/d

A = area of the graphene flake between hall bars
= 14.86 * 5.94 μm^2 = 88.26 μm^2
d = thickness of SiO_2 = 300 nm

ε = kϵ
k $\rightarrow$ dielectric constant of SiO_2 = 3.9
$\epsilon \rightarrow$ permittivity of free space = 8.85 *10^{-12} F/m
ε = 34.515*10^{-12} F/m

$\Rightarrow$ C = 88.26 * 34.515 *10^{-12}/(300) *10^{-3} F
= 10.15 * 10^{-15} F

$\Rightarrow \mu$ = 36/(10.15 * 10^{-15}) * 200 μm^2/F * μS/V
= 4.958 *10^{15} * 10^{-12} *10^{-6} * 10^4 $cm^2 V^{-1} s^{-1}$
= 7093.59 $cm^2 V^{-1} s^{-1}$.